INTERNATIONAL JOURNAL OF HYDROGEN ENERGY 41 (2016) 22043–22054

Available online at www.sciencedirect.com

ScienceDirect

journal homepage: www.elsevier.com/locate/he

CO-PrOx over nano-Au/TiO_2: Monolithic catalyst performance and empirical kinetic model fitting

M. Susana Moreno [a,*], Eduardo López [a], M. Esperanza Adrover [a], Nuria J. Divins [b], Jordi Llorca [b]

[a] PLAPIQUI – Planta Piloto de Ingeniería Química, UNS, CONICET, Camino La Carrindanga km 7, 8000, Bahía Blanca, Argentina

[b] Institut de Tècniques Energètiques and Centre for Research in Nanoengineering, Universitat Politècnica de Catalunya, Diagonal 647, ed. ETSEIB, 08028, Barcelona, Spain

ARTICLE INFO

Article history:
Received 24 June 2016
Received in revised form
19 August 2016
Accepted 21 August 2016
Available online 12 September 2016

Keywords:
CO-PrOx
Au/TiO_2 structured catalyst
Parameter estimation
Confidence intervals
Confidence regions

ABSTRACT

In this work, the performance of ceramic monoliths washcoated with Au/TiO_2 is studied on CO preferential oxidation (CO-PrOx) reaction in H_2-rich environments under a wide range of operating conditions of practical interest. The parameter estimation of a nonlinear kinetic empirical model representing this system is made via genetic algorithms by fitting the model predictions against our laboratory observations. Parameter uncertainty leading to inaccurate predictions is often present when kinetic models with nonlinear rate equations are considered. Here, after the fitting was concluded, a statistical study was conducted to determine the accuracy of the parameter estimation. Activation energies of *ca.* 30 kJ/mol and 55 kJ/mol were adjusted for CO and H_2 oxidations, respectively. The catalyst showed appropriate activity and selectivity values on the CO oxidation on a H_2-rich environment. After *ca.* 45 h on stream the catalyst showed no deactivation. Results show that the model is suitable for reproducing the behavior of the CO-PrOx reactions and it can be used in the design of reactors for hydrogen purification.

Introduction

Power consumption requirement in nowadays electronics and electrical utilities moved researchers towards the implementation of fuel cells systems with improved efficiencies. Specifically, PEM-type fuel cells are preferred for reduced-scale equipment. These units require as feed a hydrogen stream with extremely low levels of carbon monoxide to avoid the poisoning of the platinum catalyst of the fuel cell anode. In this frame, the preferential oxidation of CO in a H_2-rich atmosphere over an appropriate catalyst appears attractive due to its fairly simple implementation, lower operation costs, and minimal loss H_2 [1].

As the oxidation of carbon monoxide (Eq. (1)) competes here with the oxidation of H_2 (Eq. (2)), it is mandatory to develop highly selective catalysts. To this aim, many catalyst formulations have been studied including metal oxides (e.g., CuO–CeO_2) and noble metals (Au, Pt, Ru, Rh, and Ir) [2]. Ru is known to be also active for CO_2 methanation and can be readily deactivated upon exposure to oxygen-containing stream. Rh and Ir catalysts are less selective than Ru catalysts and seldom considered for this application [2]. The

* *Corresponding author*. Fax: +54 0291 4861600.
E-mail address: smoreno@plapiqui.edu.ar (M.S. Moreno).
http://dx.doi.org/10.1016/j.ijhydene.2016.08.136

platinum group metals supported on reducible metal oxides exhibit good performance. However, the requirement for high temperatures and the insufficient control over the unwanted conversion of H_2 have been the main drawbacks associated with the platinum group metal catalysts. On the other hand, supported gold catalysts exhibit very high performance for low-temperature CO oxidation, provided the gold is present in particles of a few nanometers [3].

$$CO + ½\ O_2 \rightarrow CO_2 \quad (1)$$

$$H_2 + ½\ O_2 \rightarrow H_2O \quad (2)$$

In addition to the size of the gold particles, the catalytic activity of supported gold catalysts is recognized to be dependent on the support [3]. Since TiO_2 is almost inert as a catalyst for CO oxidation as is bulk gold, the Au–TiO_2 system can be regarded as the most clear-cut example for investigating the significant synergistic effect between gold and the metal oxide support [4]. Many studies have demonstrated the remarkable catalytic properties of gold nanoparticles supported on TiO_2 particles for selective CO oxidation in H_2-rich streams [5–10]. Moreover, it has been addressed that Polyaniline (PANI) assembled Au/TiO_2 catalyst (Au/TiO_2–PANI) exhibited a higher activity of CO preferential oxidation than the Au/TiO_2 without PANI at room temperature under visible light irradiation [11].

Oxide-supported gold nanoparticles have been pointed as highly active and selective for preferentially eliminate carbon monoxide in H_2-rich environments at temperatures similar to those of the fuel cell (PEM-type, around 80 °C) [12]. In this way, the integration of the PrOx reactor and the fuel cell into the same cooling circuit becomes straightforward. This represents a clear advantage over the classic PrOx reactors based on Pt catalysts, whose optimum operation temperatures of around 200 °C lays in between the temperature of the reactor upwards (usually shift reactors at *ca.* 400 °C) and the fuel cell.

In addition to a highly selective catalyst, reactor design and determination of operation conditions are critical aspects that have to be addressed. Research is also concerned with applying and evaluating non-conventional reactors such as microreactors and monolith reactors [13]. However, studies on structured catalyst for this reaction are scarcer and even more those studies restricted to cordierite monolithic catalysts [14–19].

Reaction rates adequately representing both competing oxidation reactions appear mandatory towards the implementation of a mathematical model of the PrOx reactor. There are many papers that report rate expressions for CO oxidation for different catalytic systems as Pt/γ-Al_2O_3 [20–22], Cu–CeO [23], Au/TiO_2 [24,25]. However, only few works consider H_2 oxidation simultaneously with CO oxidation [26]. Even fewer rate expressions for both competitive reactions, i.e., H_2 oxidation and CO oxidation over Au-based catalysts can be found in literature. Kahlich et al. [12] concluded that the kinetics of selective CO oxidation over Au/α-Fe_2O_3 can be expressed by a power law functionality and that the reaction rates of CO and H_2 oxidations are not interrelated. López et al. [27] proposed power law expressions for CO and H_2 oxidation whose kinetic parameters were fitted from experiences carried out in an isothermal flat-bed reactor filled with Au/α-Fe_2O_3-γ-Al_2O_3 pellets. Laguna et al. [28] carried out a kinetic study for the CO-PrOx reaction over AuCeCu and CeCu catalysts disposed in a micro-packed bed and assuming a Langmuir-Hinshelwood type expression for CO oxidation and a power–law type expression in the case of H_2 oxidation.

There exist a variety of numerical optimization methods to solve the estimation problem related to the unknown parameters of the rate expressions. These techniques have been grouped in deterministic and stochastic ones depending whether they use derivative information or not. Among the stochastic approaches, the Genetic Algorithm (GA) is one of the most popular because this optimization technique tends to find the global optimum solution without becoming stuck at local minima [29]. Several authors have resorted to GAs for tackling the parameter estimation problem [30–32].

Parameter uncertainty leading to inaccurate predictions is often present when kinetic models with nonlinear rate equations are considered. In nonlinear estimation problems, after a solution has been found, an assessment of the parameter values should be performed in order to estimate their uncertainties in rigorous statistical terms [33], including the estimation of the confidence intervals, the joint confidence region, and the correlations between the fitted parameters.

This work aims at evaluating the performance of the gold-based structured catalyst on the CO-PrOx reaction. The kinetic parameters of an empirical nonlinear model were estimated using a GA technique. For making the model calibration, we use our own experimental observations in a lab scale unit and under a well-defined range of operating conditions of practical interest. Furthermore, in order to assess the quality of the kinetic parameters obtained from the fitting, an identifiability analysis has been performed.

Experimental

Catalyst preparation and characterization

Two types of conventional cordierite monoliths were chosen as support for the gold-based catalyst. First and aiming the generation of kinetic data over which the parameter estimation is based, we prepared two cylindrical pieces with square cross-section of side *ca.* 0.5 mm (900 cpsi), having 1.4 cm of length and 1.4 cm of diameter each. A homogeneous TiO_2 layer was deposited over the monolith walls using titanium isopropoxide (Panreac) as precursor. The samples were dried under continuous rotation for 1 h at 353 K and then calcined at 723 K for 4 h (1 K min^{-1}). Pre-formed gold nanoparticles, obtained by the two phase transfer method [34], were grafted afterwards onto the TiO_2 support (2% w/w) by calcination at 673 K for 2 h (2 K min^{-1}) [35]. Additionally, an extra cordierite monolithic sample was functionalized with the same method aforementioned to perform experiences to validate the kinetics obtained after the fitting procedure. This last monolith comprises 400 cpsi (square channels of 1 mm side) and measures 2 cm length and 2 cm diameter. Before experiences, samples were activated under reaction mixture at 473 K for

2 h. Detailed characterization results of the prepared catalysts have been already reported by the authors in a previous paper [35]. Here, we characterized the catalytic monoliths with scanning electron microscopy (SEM) and high-resolution transmission electron microscopy (HRTEM) to study the morphology and structure of the catalytic layer. SEM was conducted with a Zeiss Neon40 Crossbeam Station equipped with a field emission electron source and HRTEM was carried out with a JEOL 2010 instrument at 200 kV.

Reaction set-up

CO preferential oxidation experiences were conducted in a conventional lab facility, as shown in Fig. 1. The two functionalized monolithic samples of 900 cpsi and 1.4 × 1.4 cm length and diameter were sealed into a stainless steel housing. The reactor was disposed inside an electric furnace (Heraheus) governed with a PID electronic controller (Novus 480D). A K-type thermocouple was additionally used to register the reactor temperature. The feed process stream to the reactor resembled the composition exiting a shift reactor (dry mixture, 1.41% CO, 24.33% CO_2, balance H_2). Air is used to provide the required oxygen. Both gas streams were dosed by using two independent mass flow controllers (Brooks). Exit compositions of reactants, products, and inerts (CO, CO_2, H_2, O_2 and N_2) were quantified by GC (HP 4890, Molsieve 5 Å and Porapak-Q packed columns, TCD detector). To close element balances, the total volumetric flowrate of the outlet gas stream was measured (bubble soap meter). Water condensed from the reactor (formed by the undesired hydrogen oxidation) was collected in an appropriate vessel.

Operating conditions and performance parameters

The lab facility presented in Fig. 1 allowed steady-state measurements of the catalyst performance under isothermal/isobaric conditions; the operating conditions are reported in Table 1. A constant pressure of 1.2 bar (absolute) was adopted for all tests, in accordance to the operation conditions of a PEM type fuel cell. 2–4 replica of each measurement showed appropriate reproducibility. 40 different experiences were performed, amounting 160 experimental observations (as molar flowrates of CO, CO_2, H_2, and O_2 leaving the reactor). By closing element balances, water contents were calculated in the reactor exit. Catalyst showed no deactivation signs after *ca.* 45 h on stream.

Table 1 – Experimental conditions.

Temperature (K)	334–403
Pressure (bar)	1.2
Feed load (WHSV) (ml/g_{cat} min)	45–375
Feed concentration (λ, Eq. (5)) (mol_{O_2}/mol_{CO})	0.4 (0.8)–4.1 (8.2)

To quantify the catalyst performance towards the CO-PrOx reaction, both the CO conversion (x_{CO}) and the reaction selectivity (S) were calculated by using Eqs. (3) and (4). The reaction selectivity is calculated as the quotient of the oxygen flowrate used to only oxidize CO to CO_2 and the total oxygen consumption (i.e., oxidations of both CO and H_2).

$$x_{CO} = \frac{(F^0_{CO} - F_{CO})}{F^0_{CO}} \tag{3}$$

$$S = \frac{(F^0_{CO} - F_{CO})}{2\left(F^0_{O_2} - F_{O_2}\right)} \tag{4}$$

The parameter λ, as defined by Eq. (5), is commonly used in CO-PrOx to quantify the oxygen excess in feed, where $\lambda = 1$ is the stoichiometric relation to only oxidize the CO fed.

$$\lambda = \frac{2\,F^0_{O_2}}{F^0_{CO}} \tag{5}$$

Theoretical framework

The inverse problem & statistical evaluation

The fitting procedure of the kinetic parameters is also referred as an inverse problem. Here, results arisen from a mathematical model expressed by a set of differential-algebraic

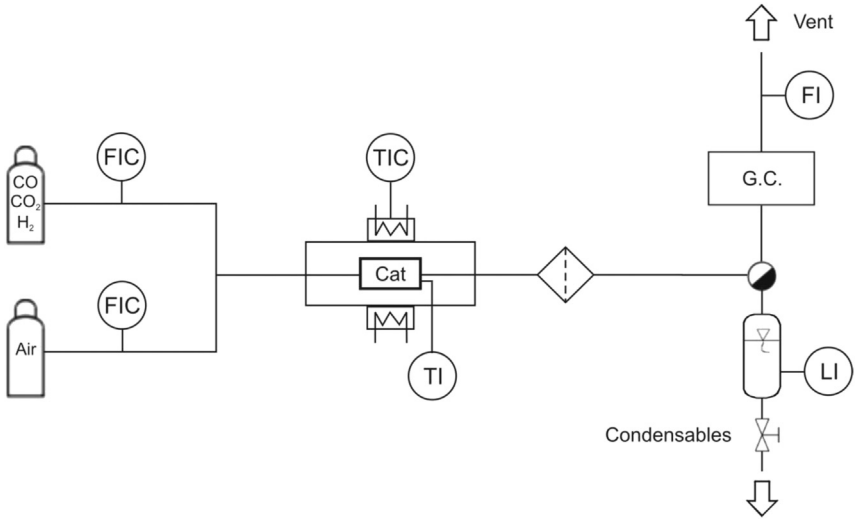

Fig. 1 – Experimental set-up.

equations (DAEs) are contrasted with experimental observations of the performance of the CO-PrOx reaction over the prepared monolithic catalyst [36]. The fitting problem can be mathematically expressed as:

$$\min J(\mathbf{p}) = \left(\mathbf{x}^{e} - \mathbf{x}^{*}\right)^{T} \mathbf{V}^{-1} \left(\mathbf{x}^{e} - \mathbf{x}^{*}\right) \tag{6a}$$

s.t.

$$\frac{d\mathbf{x}}{dz} = \mathbf{f}(\mathbf{x}, \mathbf{u}, \mathbf{p}, z) \tag{6b}$$

$$\mathbf{h}(\mathbf{x}, \mathbf{u}, \mathbf{p}, z) = \mathbf{0} \tag{6c}$$

$$\mathbf{x}(z^{0}) = \mathbf{x}^{\mathbf{0}},\ z \in [z^{0},\ z^{f}] \tag{6d}$$

$$\mathbf{x}^{L} \leq \mathbf{x} \leq \mathbf{x}^{U} \tag{6e}$$

$$\mathbf{p}^{L} \leq \mathbf{p} \leq \mathbf{p}^{U} \tag{6f}$$

where $J(\mathbf{p})$ is the objective function to be minimized, $\mathbf{p}$ are the parameters (decision variables of the problem), $\mathbf{x}^{e}$ are experimental measurements of differential state variables, $\mathbf{x}^{*}$ are model predictions of those variables, $\mathbf{V}$ is a weighting matrix, $\mathbf{u}$ are the algebraic variables, z represents the axial coordinate, $\mathbf{f}$ are the differential constrains whereas $\mathbf{h}$ are the algebraic ones.

As already referenced, a Genetic Algorithm (GA) method is adopted here towards the optimization problem at hand. The model (as described in Section Results and discussions) was implemented in the MATLAB 7.6.0 platform (The Mathworks, Inc.) and through the genetic algorithm option available in the optimization tool of this software the parameter estimation was carried out. More information regarding the GA approach and its implementation and use, can be found elsewhere [33,37,38].

In this contribution, once the parameters have been fitted by the GA, a statistical assessment of these estimates is performed to judge their reliability. Confidence intervals and confidence ellipsoids of $\mathbf{p}^{*}$ in nonlinear models are obtained through an approximate covariance matrix expressed as [39]:

$$\mathbf{C}(\mathbf{p}^{*}) = \frac{J(\mathbf{p}^{*})}{NE - n_{p}} \left[\left(\frac{\partial \mathbf{x}}{\partial p}(\mathbf{p}^{*}) \right)^{T} \mathbf{V}^{-1} \left(\frac{\partial \mathbf{x}}{\partial p}(\mathbf{p}^{*}) \right) \right]^{-1} \tag{7}$$

Here, $J(\mathbf{p}^{*})$ is the minimum value of the sum of the square errors calculated from the parameter estimation problem Eqs. (6) and $\frac{\partial \mathbf{x}}{\partial p}(\mathbf{p}^{*})$ represents a sensitivity matrix of model variables $\mathbf{x}$ with respect to the parameter estimations. Also, quantities NE and n_p are the number of experiments and adjusted parameters, respectively.

Using the $\mathbf{C}(\mathbf{p}^{*})$ matrix, computed via the Fisher Information Matrix, the approximate confidence intervals in $\mathbf{p}$ space can be determined by Eq. (8) [40,41].

$$\left\{ \mathbf{p} : (\mathbf{p} - \mathbf{p}^{*})^{T} \mathbf{C}^{-1} (\mathbf{p} - \mathbf{p}^{*}) \leq n_{p} F^{1-\alpha}_{n_{p}, NE-np} \right\} \tag{8}$$

where $F^{1-\alpha}_{n_p, NE-np}$ is the value from the F distribution with (NE-n_p) degrees of freedom and ($1-\alpha$) represents a given confidence level.

The confidence interval of each parameter m, δ_m, is quantified by:

$$\delta_{m} = \pm t^{1-(\alpha/2)}_{NE-n_{p}} \sqrt{C_{mm}} \tag{9}$$

where $t^{1-(\alpha/2)}_{NE-n_p}$ is the t-distribution value corresponding to the (α/2) percentile and C_{mm} are the elements in the main diagonal of matrix $\mathbf{C}(\mathbf{p}^{*})$.

The approximate correlation coefficients between two estimated parameters (Q_{ml}) indicate the strength of their correlation. Therefore, $Q_{ml} = 0$ indicates no correlation at all between fitted parameters, on the other hand $Q_{ml} = 1$ means unidentifiable parameters. Individual coefficients Q_{ml} are calculated here using the following equation:

$$Q_{ml} = \frac{C_{ml}}{\sqrt{C_{mm} C_{ll}}} \tag{10}$$

Model formulation

A 1-D pseudo-homogeneous mathematical model was implemented to represent the steady-state operation of the Au/TiO_2 monolithic catalyst described in previous sections. Isothermal and isobaric operation was assumed. This model was profited in the kinetic parameter fitting procedure. The following mass balance equations were considered for each specie j present in the reaction medium:

$$\frac{dF_{j}}{dz} = \rho_{B}\, A_{T} \sum_{i=1}^{M} \upsilon_{ij}\, r_{i} \quad \forall\, j \tag{11}$$

In Eq. (11), F_j is the molar flowrate of component j (mmol min^{-1}), A_T represents the cross sectional area of monolith (m^2), ρ_B is the catalyst loading ($g_{cat}\ m^{-3}$), υ_{ij} is the stoichiometric coefficient of component j in reaction i, and r_i is the reaction rate of i (mmol $g_{cat}^{-1}\ min^{-1}$).

Reaction rates for CO and H_2 oxidations (Eqs. (1)–(2)) are represented here by power-law type expressions:

$$r_{1} = k_{1}\, p_{CO}^{n_{1}}\, p_{O_{2}}^{n_{2}} \tag{12}$$

$$r_{2} = k_{2}\, p_{H_{2}}^{n_{3}}\, p_{O_{2}}^{n_{4}} \tag{13}$$

$$k_{i} = k_{i}^{0} \exp\left(-\frac{E_{i}}{RT}\right) \quad \forall\, i \tag{14}$$

where p_j are partial pressures of species j (bar), n_j are the reaction orders, k_i^0 is the pre-exponential constant (mmol $g_{cat}^{-1}\ min^{-1}\ bar^{-n}$), E_i is the activation energy (kJ mol^{-1}), R being the universal gas constant (8.3144×10^{-3} kJ $mol^{-1}\ K^{-1}$), and T represents the temperature (K).

Partial pressures p_j and molar flowrates F_j are related via Eq. (15) where P represents the total pressure (bar).

$$p_{j} = \frac{F_{j}}{\sum_{j} F_{j}} P \quad \forall\, j \tag{15}$$

It's well known that external and/or internal mass transfer phenomena can play an important role in the observed reaction rate [42]. However, one of the great advantages on the using of microchannel reactors is based on the fact that only small temperature and concentration gradients are to be expected [43]. Different criteria were applied in order to evaluate the absence of external and internal mass gradients affecting the estimation of reaction rates. In the case of CO-PrOx, two

reactions are involved, i.e., oxidations of CO and hydrogen. It is common practice to select the fastest reaction under the system conditions to evaluate the mentioned criteria [44,45].

The Weisz–Prater criterion can be selected to asses if internal mass transport limitations affect the reaction rate of an irreversible reaction. The Weisz–Prater criterion adapted for the geometry of a flat catalyst layer was applied here [46]. In the present case, a porous TiO_2 catalyst layer of 30 μm (see Section Catalytic monolith characterization) deposited over the monoliths walls leads to fulfillment of the Weisz–Prater criterion allowing to conclude that intraparticle mass resistances can be neglected.

Although most commonly the principal mass transfer resistance occurs inside the particle [45], a modified Mears criterion to wall coated microreactors was applied here to evaluate the contribution of external mass transfer resistances [43]. For the operating and geometrical conditions selected in this study, the Mears criterion allowed us to neglect the explicit evaluation (i.e., the use of a heterogeneous model) of the mass transfer phenomenon in the boundary layer, even under conditions of maximum conversion.

The objective function minimized along the fitting procedure was:

$$\min J(\mathbf{p}) = \sum_{e=1}^{NE}\sum_{j=1}^{NC}\left(\frac{F_{ej}-F_{ej}^{*}}{\max(F_{ej})}\right)^{2} \quad (16)$$

where F_{ej} and F_{ej}^{*} are the experimental and calculated exit molar flowrates of component j in the experiment e, respectively. NE represents the number of experiments ($NE = 200$) and NC the total number of components considered ($NC = 5$). In Eq. (16), $\max(F_{ej})^{-2}$ corresponds to weights used for normalizing the contribution of each term.

To sum up, the fitting problem addressed in this work corresponds to a DAE system composed by 5 differential equations (Eq. (11)) and 2 algebraic equations (Eqs. (12)–(13)). In this way, the problem considers 5 state variables and 8 parameters (k^{0}'s, E's, and n's) to be fitted.

Results and discussions

Catalytic monolith characterization

The catalytic layer deposited onto the monolith walls was characterized by electron microscopy (Fig. 2). As evidenced by SEM, the deposition of the TiO_2 catalyst support formed a homogeneous layer of about 30 μm in thickness over the monolith walls (Fig. 2b). SEM images also showed the porous structure of the monoliths. The structure of the Au/TiO_2 catalytic layer was characterized in detail by HRTEM. Nanometer-sized Au nanoparticles were identified over the TiO_2 support and were well-distributed. As a representative example, in Fig. 2c lattice fringes corresponding to TiO_2 in its anatase polymorph were identified at 3.52 Å, which are ascribed to the characteristic (101) crystallographic planes (see the corresponding Fourier Transform image in the inset). Also, an individual Au nanoparticle was identified, which was oriented along the [100] crystallographic direction. Spots at 2.04 Å in the corresponding Fourier Transform image corresponded well to the (200) planes of metallic Au. Therefore, we conclude that the monoliths were successfully coated with an homogeneous layer of Au/TiO_2 catalyst, with Au nanoparticles well distributed over anatase, as expected.

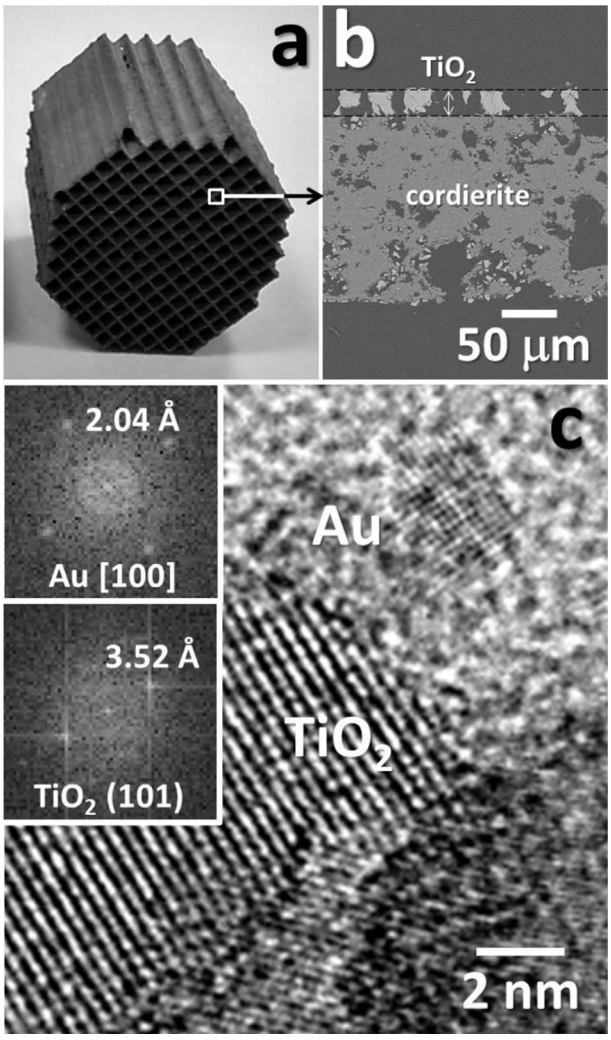

Fig. 2 – (a) Photograph of the 400 cpsi monolith used coated with Au/TiO_2 catalyst. (b) SEM image of a cross section of a polished monolith wall showing the porous structure of the cordierite support and the catalytic layer. (c) HRTEM image of the Au/TiO_2 catalyst.

Parameter estimation and identifiability analysis

This section is devoted to the study, by means of a statistical evaluation, of the goodness of the fitting procedure via a reliable identification of the adjusted kinetic parameters in Eqs. (12)–(14). As stated before, the nonlinear problem was implemented and solved using GA in the MATLAB software. For the algorithm, the stopping criterion considered here was a maximum number of generations of 100 or a cumulative change in the objective function value less than 1×10^{-9} over 50 stall generations, whichever occurs first.

Table 2 reports the fitted values of the kinetic parameters along with their correspondent 95% confidence intervals (CI)

Table 2 – Estimated kinetic parameters, 95% confidence intervals (CI), and correlation coefficients (significant correlations highlighted in bold).

p	Value	95% CI	Correlation matrix							
			k_1^∞	E_1	k_2^∞	E_2	n_1	n_2	n_3	n_4
k_1^∞	4.36×10^7	$\pm 3.25 \times 10^7$	1.00							
E_1	29.24	±0.98	**0.79**	1.00						
k_2^∞	3.64×10^8	$\pm 6.88 \times 10^7$	0.44	0.70	1.00					
E_2	55.42	±0.39	0.47	**0.77**	**0.94**	1.00				
n_1	1.30	±0.08	**0.89**	0.45	0.12	0.14	1.00			
n_2	1.13	±0.04	**0.87**	0.55	0.31	0.30	**0.76**	1.00		
n_3	1.20	±0.08	0.34	0.45	**0.82**	0.63	0.18	0.19	1.00	
n_4	0.70	±0.01	0.22	0.40	**0.83**	0.62	−0.04	0.29	**0.79**	1.00

which quantify the uncertainty of the individual fittings. Table 2 also shows the correlation matrix where only the 10 × 10 lower triangular matrix is displayed. Bold values indicate the few pronounced correlations between pairs of parameters (values > 0.7).

Parameter estimations have narrow confidence intervals indicating sufficient amount of experimental observations. These narrow confidence bands reduce parameters uncertainty. The normalized covariance matrix presented in Table 2 possesses many weakly correlated parameters which can therefore be simultaneously estimated by least square optimization.

Fitted values for the activation energies of both competing reactions agree well with reports in the literature when the preferential oxidation of carbon monoxide in hydrogen-rich environments conducted over Au/TiO_2 catalysts is considered [27,46]. A fitted E_1 of *ca.* 30 kJ/mol points the superior performance of nanosized gold towards CO oxidation at reduced temperatures. Moreover, the difference between the achieved values of E_1 and E_2 ($E_1 < E_2$) confirms experimental observations regarding selectivity losses as T increases. This fact should be on the focus when the design of the CO-PrOx reactor is accomplished: the heat of reaction (both oxidation reactions present elevated exothermicity) has to be efficiently removed from the reaction chamber to prevent undesired operation with reduced selectivity, which renders unconverted CO and excessive H_2 losses.

Parity plots reporting a comparison between experimental and simulated exit flowrates (all experiences) are depicted in Fig. 3. As shown, not any systematic deviations are observed, with the points reasonably spread around the diagonal line.

Fig. 4 presents confidence regions corresponding to 99, 95 and 90% confidence levels for selected pairs of estimated parameters as a picture of the quality of the fitting performed.

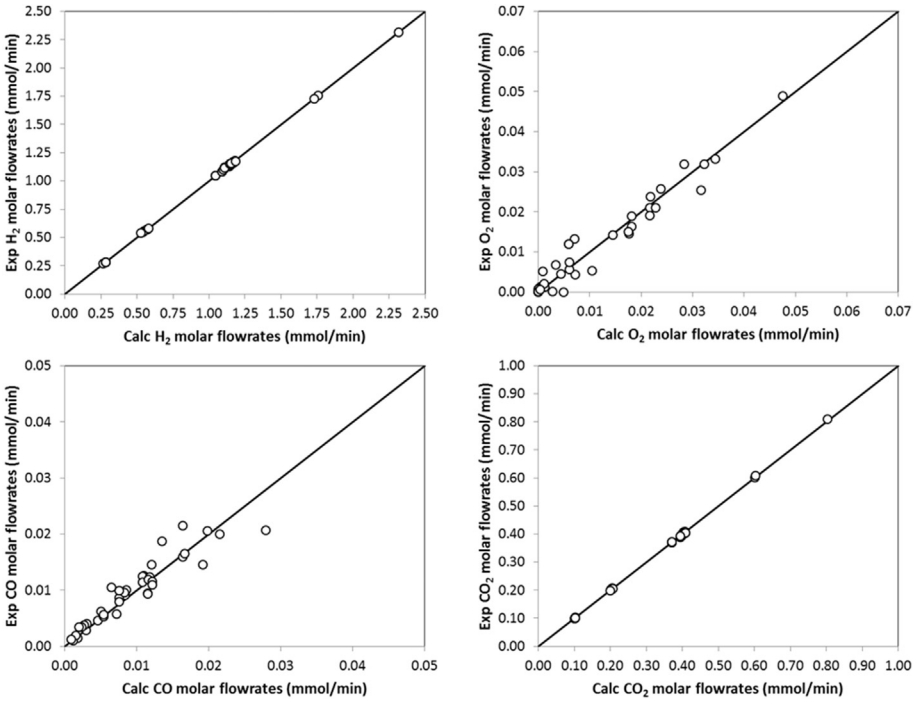

Fig. 3 – Measured vs. calculated exit flowrates for each component considering the parameters reported in Table 2.

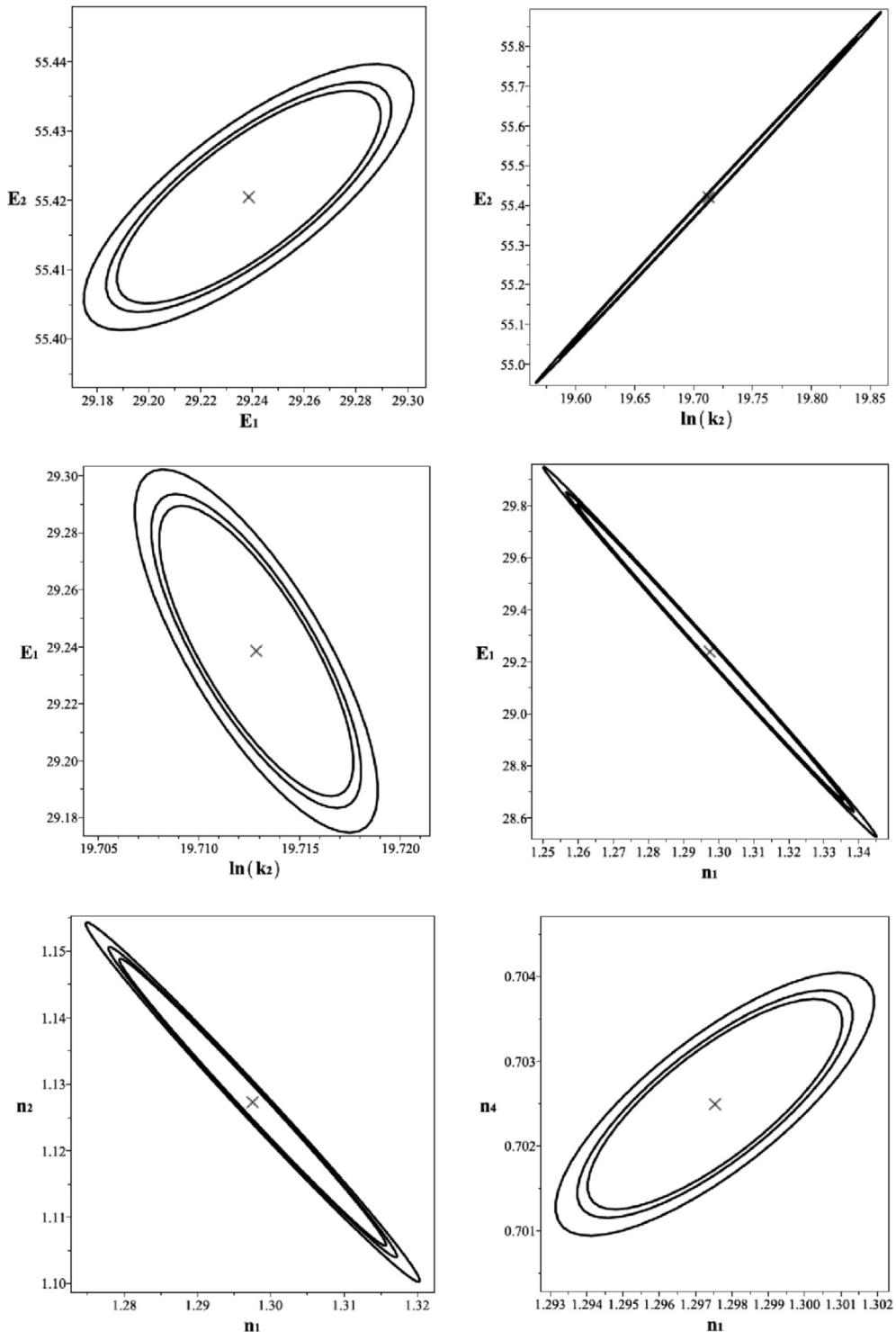

Fig. 4 – Ellipsoids considering 99, 95, and 90% confidence levels. The symbol (×) indicates the parameter values obtained by the optimization algorithm.

The narrow shapes of the ellipses indicate a reliable estimation of the parameters.

Reaction performance

The influence of different operating variables, i.e., oxygen excess (λ), total inlet flowrate (F_{TO}) and temperature (T) on catalytic performance is analyzed in the present section. Additionally to the experimental results employed to fit the mathematical model, modeling results are also included in the following figures. The inlet reaction mixtures of the experiences presented in this section consisted in 66% H_2, 1.3% CO (13,000 ppm), 1–4.5% O_2, 21% CO_2 and the corresponding N_2 of the air in feed (*ca.* 8%).

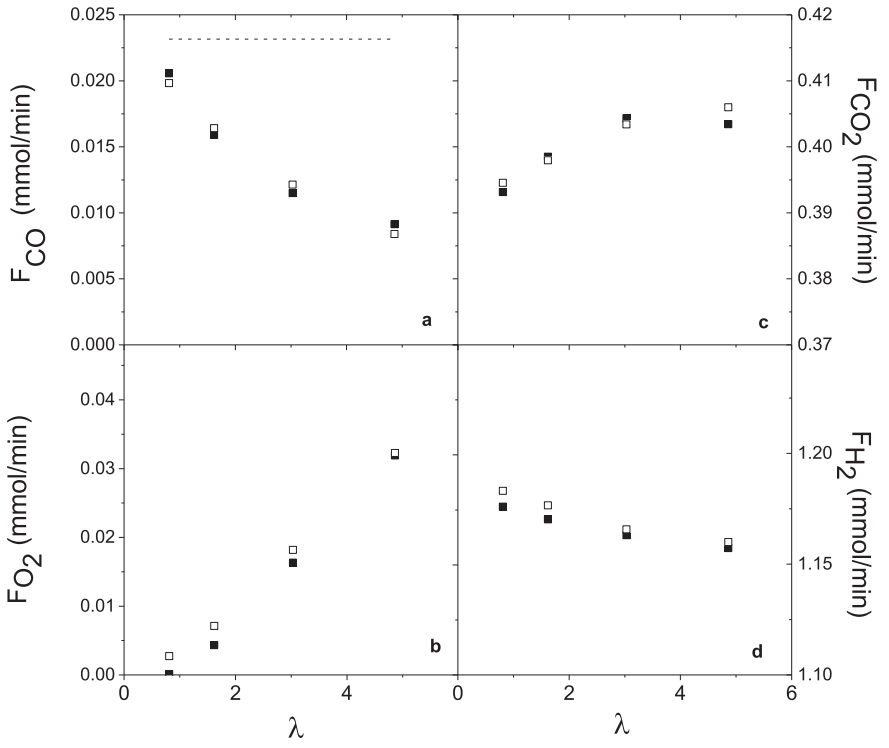

Fig. 5 – Influence of λ over (a, b) reactants and (c, d) products outlet flowrates: ■ experimental and □ model results. T = 363 K, WHSV = 174–206 (ml/g_{cat} min) Fig. 5a: (----) represents inlet CO molar flowrate.

Fig. 5 illustrates the behavior of reactants and products outlet flowrates for different λ values. Fig. 5a shows that as λ is increased, more CO is converted and consequently lower CO outlet flowrates and higher CO_2 amounts are obtained, with a constant CO feed flowrate, which is represented in Fig. 5a with a dashed line. However, the increased O_2 available in the reaction mixture promotes undesired H_2 consumptions in the monolith. This O_2 surplus in the reactor entrance is also evidenced as higher amounts of unconverted O_2 leaves the reactor. Although a temperature as low as 363 K was selected for experiences in Fig. 5, a maximum CO conversion of 60% was achieved reflecting an enhanced ability of the Au/TiO_2 functionalized monoliths to conduct the CO-PrOx reaction in a

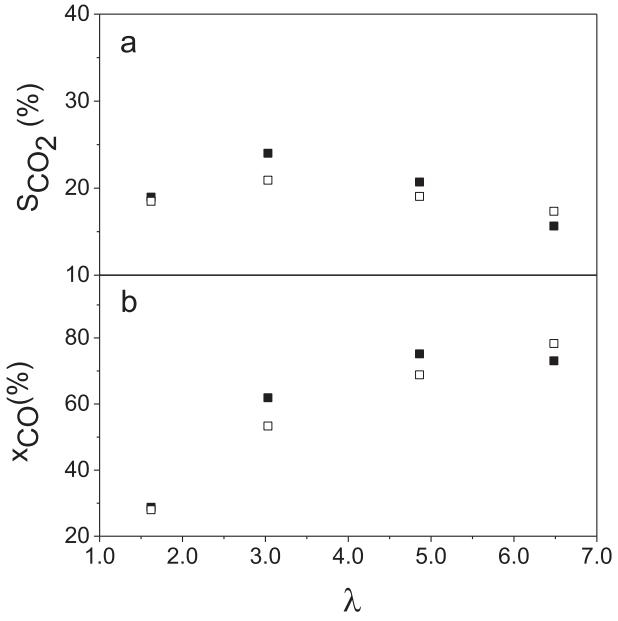

Fig. 6 – Influence of λ over (a) CO_2 selectivity (S_{CO_2}) and (b) CO conversion (x_{CO}): ■ experimental and □ model results. T = 383 K, WHSV = 178–206 (ml/g_{cat} min).

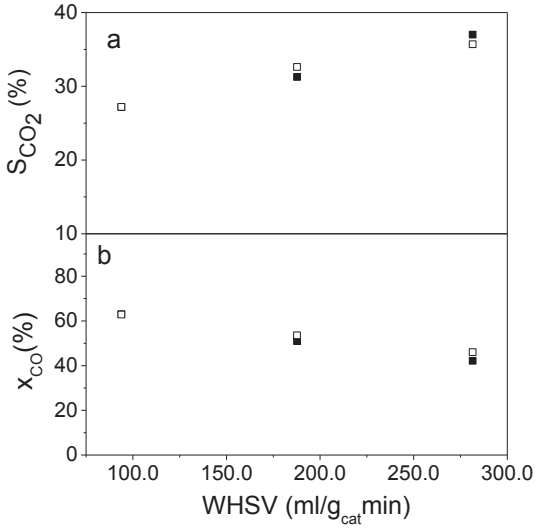

Fig. 7 – (a) CO_2 selectivity (S_{CO_2}) and (b) CO conversion (x_{CO}) as a function of WHSV: ■ experimental and □ model results. T = 363 K, λ = 3.

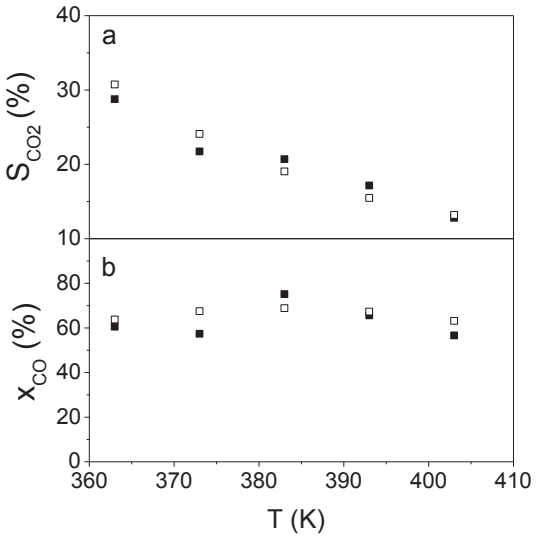

Fig. 8 – Temperature effect over (a) CO_2 selectivity (S_{CO_2}) and (b) CO conversion (x_{CO}). ■ experimental and □ model results. $\lambda = 5$, WHSV = 197 (ml/g_{cat} min).

hydrogen-rich environment. It is also worth mentioning that model results satisfactorily reproduce experimental measurements.

Fig. 6 reports results of the influence of λ on the catalytic performance. As previously observed for Fig. 5, as λ is increased more O_2 is available to oxidize the CO and, consequently, CO conversion increases. Therefore, selectivity to CO_2 drops as λ shifts from 3 to 6.5 as a consequence of lower mean CO concentrations along the reactor. This effect is in accordance with the adjusted kinetic parameters. In fact, although adjusted reaction orders for CO and H_2 (1.13–0.7, respectively) would indicate an increase in the ratio between CO and H_2 oxidation rates as oxygen partial pressures augments, the CO depletion effect at almost constant H_2 partial pressure (due to the huge H_2 excess) impact in a definitive way over the observed selectivity. It should be noted a reduced S_{CO_2} value for $\lambda = 1.5$ as O_2 was depleted here within the reactor. CO conversions of *ca.* 80% were achieved here operating at a temperature level 20 K higher than the experiences presented in Fig. 5.

It is worth remarking that the influence of the reverse or direct water-gas shift reaction should be neglected here due to the low operation temperatures at hand.

Results regarding CO_2 selectivity and CO conversion are presented as affected by the feed flowrate in Fig. 7. As expected, WHSV increases implying reduced residence times lead to lower CO conversions. Again, higher mean CO molar fractions along the reactor are associated with higher observed selectivity values.

The effect of the operating temperature over both CO conversion and CO_2 selectivity is addressed in Fig. 8. As shown in this figure, CO conversion does not present a monotonous behavior with temperature. In fact, temperature increments from low values lead to an increase in conversion based on kinetic reasons, achieving a high conversion value of 79% at T = 383 K. On the other hand, as temperature increases further ($T \geq 383$ K in this case) the selectivity deteriorates in such an extent and the O_2 is preferentially consumed by the non-desired H_2 oxidation, rendering enhanced amounts of unconverted CO. This behavior obeys to the fact that the

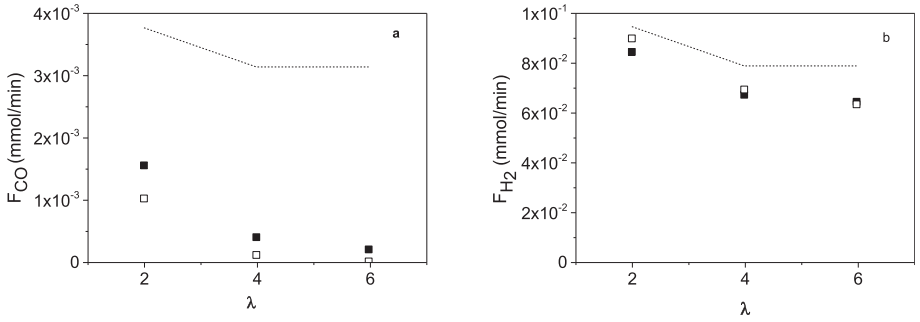

Fig. 9 – Influence of λ over (■) experimental and (□) calculated exit CO (a) and H_2 (b) molar flowrates, (----) represents inlet CO molar flowrates. T = 363 K. Feed mixture: 50% H_2, 2% CO (20,000 ppm), 2–6% O_2, and N_2 as balance.

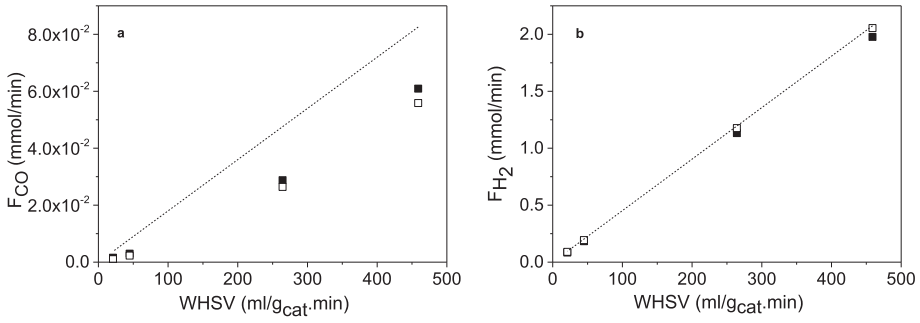

Fig. 10 – Influence of the feed load over (■) experimental and (□) calculated exit CO (a) and H_2 (b) molar flowrates. (----) represents inlet CO molar flowrates. T = 363 K, $\lambda = 2$. Feed mixture: 50% H_2, 2% CO (20,000 ppm), 2% O_2, and N_2 as balance.

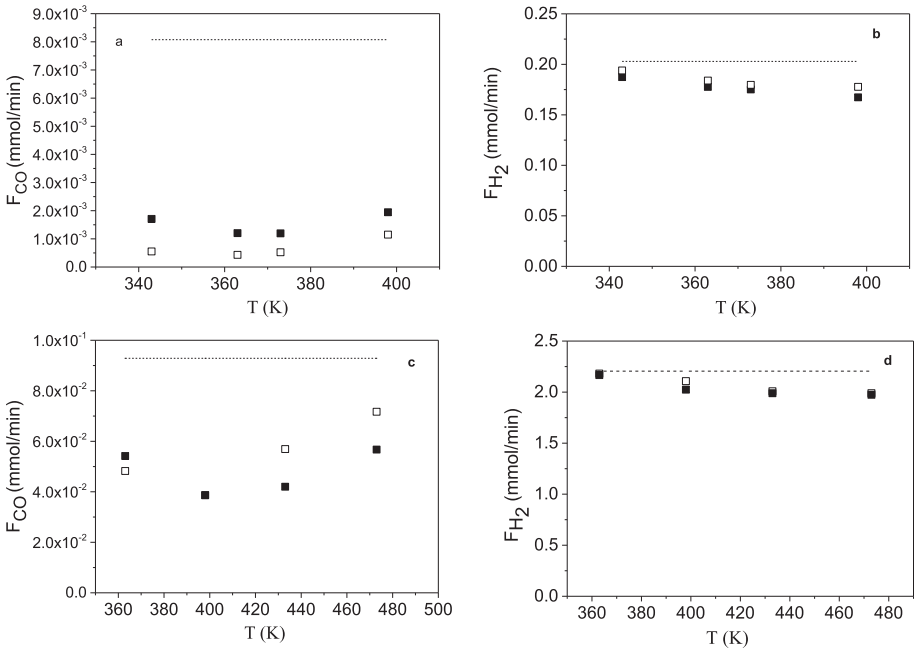

Fig. 11 – Temperature effect over (■) experimental and (□) calculated exit CO (a, c) and H_2 (b, d) molar flowrates. (----) Inlet flowrates. Feed mixture: 50% H_2, 2% CO (20,000 ppm), 2% O_2, and N_2 as balance. (a, b): $\lambda = 4$, WHSV = 45 (ml/g_{cat} min). (c, d): $\lambda = 2.7$, WHSV = 498 (ml/g_{cat} min).

activation energy of H_2 oxidation is higher than that of the CO oxidation, as reported elsewhere for CO-PrOx over gold-based catalysts [28].

It is important to remark that model results satisfactorily reproduces the experimental results presented in this section.

Model validation

The adequacy of the calibrated model is assessed by confronting its predictions with experimental data not used to estimate the parameters of the model. Experiences presented here were performed with the same Au/TiO_2 catalyst studied in Section Reaction performance (900 cpsi monoliths) but now washcoated over 400 cpsi cordierite monoliths (see Section Catalyst preparation and characterization) and using a lab facility similar to that presented in Fig. 1. An extended temperature range from that presented in Table 1 was studied; additionally, some differences in the reactor feed were selected as no CO_2 was included and pure O_2 instead of air was used (now N_2 acts as balance). The influence of λ, feed load, and operating temperature on both observed and calculated exit CO flowrates is presented in Figs. 8–10, respectively. These figures show that exit CO flowrates follow similar trends with operational variables as those already discussed in Section Reaction performance. It could be remarked here that CO conversion levels of maximum 93% in Fig. 9a and of 85% for optimum temperatures in Fig. 11a were achieved.

On the other hand, and in spite of the usage of feed loads of *ca.* one order of magnitude higher and lower values of λ, CO conversions of 60% are achieved as presented in Fig. 11c. Additionally, good predictions of the H_2 exit flowrates were possible. Summing up, and based on the comparison between model results and the experimental data presented in Figs. 8–10, it can be concluded that the fitted power-law type kinetic model proved successful in predicting the performance of gold/titania catalysts on the CO preferential oxidation in H_2-rich environments under operating conditions of practical interest.

Conclusions

The present contribution reports the estimation of kinetic parameters considering a power law–type reaction rate expression to describe lab experiences for the CO preferential oxidation process over an Au/TiO_2 structured catalyst.

The parameter estimation problem has been solved using Genetic Algorithms. The objective of the model is to minimize the weighted least squares. The estimates have been obtained using experimental results from our laboratory.

In order to investigate the precision of the adjusted parameters, an identifiability analysis has been performed. The goodness of the model fits is quite remarkable considering the wide range of experimental conditions used, i.e., different oxygen excesses (λ), total inlet flowrates (F_{TO}) and temperatures (T). Activation energies of *ca.* 30 kJ/mol and 55 kJ/mol were adjusted for CO and H_2 oxidations, respectively. The catalyst showed an appropriate activity and selectivity values on the CO oxidation on a H_2-rich environment. After *ca.* 45 h on-stream the catalyst showed no deactivation.

Additionally, the adequacy of the calibrated model was assessed by confronting its predictions with experimental data not used for estimating the parameters of the model. It can therefore be concluded that the fitted power-law type

kinetic model successfully predicts the performance of gold/titania catalysts on the CO preferential oxidation in H_2-rich environments under operating conditions of practical interest and constitutes an useful tool for CO-PrOx reactor designs.

Acknowledgment

The authors want to thank the financial support from Consejo Nacional de Investigaciones Científicas y Técnicas (CONICET) and Ministerio de Ciencia, Tecnología e Innovación Productiva (MINCyT) (MINCYT-MICINN 2011: ES/11/07) from Argentina. JL is Serra Húnter Fellow and is grateful to ICREA Academia program and MINECO/FEDER grant ENE2015-63969-R.

Nomenclature

Subscripts

e	Experiment
i	Reaction
j	Component
m	Parameter

Superscripts

L	Lower bound
U	Upper bound
0	Inlet value

Parameters

A_T	Cross sectional area of monolith, m^2
F_j	Molar flowrate of component j, mmol min^{-1}
k_i	Reaction rate constant for reaction i, min^{-1}
k_i^0	Frequency factor, mmol g_{cat}^{-1} min^{-1} bar^{-n}
NE	Number of experiments
NC	Number of components
p_j	Pressure of component j, bar
P	Total pressure, bar
r_i	Reaction rate
R	Universal gas constant, kJ mol^{-1} K^{-1}
T	Temperature, K
v_{ij}	Stoichiometric coefficient of component j in reaction i
y_j	Molar fraction of component j
ρ_B	Catalyst loading per unit monolith volume, g_{cat} m^{-3}

REFERENCES

[1] Korotkikh O, Farrauto R. Selective oxidation of CO in the presence of hydrogen fuel cell applications. Catal Today 2000;62:249–54.
[2] Wei Z, Sun J, Li Y, Datyec AK, Wang Y. Bimetallic catalysts for hydrogen generation. Chem Soc Rev 2012;41:7994–8008.
[3] Lakshmanan P, Park JE, Park ED. Recent advances in preferential oxidation of CO in H_2 over gold. Catal Surv Asia 2014;18:75–88.
[4] Tsubota S, Cunningham D, Bando Y, Haruta M. CO oxidation over gold supported on TiO_2. In: Inui T, Fujimoto K, Uchijima T, Masai M, editors. New aspects of spillover effect in catalysis. Elsevier Science Publishers B.V; 1993. p. 325–8.
[5] Bamwenda GR, Tsubota S, Nakamura T, Haruta M. The influence of the preparation methods on the catalytic activity of platinum and gold supported on TiO_2 for CO oxidation. Catal Lett 1997;44:83–7.
[6] Schumacher B, Denkwitz Y, Plzak V, Kinne M, Behm RJ. Kinetics, mechanism, and the influence of H_2 on the CO oxidation reaction on a Au/TiO_2 catalyst. J Catal 2004;224:449–62.
[7] Daté M, Haruta M. Moisture effect on CO oxidation over Au/TiO_2 catalyst. J Catal 2001;201:221–4.
[8] Galletti C, Fiorot S, Specchia S, Saracco G, Specchia V. Catalytic performance of Au-TiO_2 catalysts prepared by deposition-precipitation for CO preferential oxidation in H_2-rich gases. Chem Eng J 2007;134:45–50.
[9] Kipnis M. Gold in CO oxidation and PROX: the role of reaction exothermicity and nanometer-scale particle size. Appl Catal B Environ 2014;152–153:38–45.
[10] Yang K, Liu J, Si R, Chen X, Dai W, Fu X. Comparative study of Au/TiO_2 and Au/Al_2O_3 for oxidizing CO in the presence of H_2 under visible light irradiation. J Catal 2014;317:229–39.
[11] Yang K, Li Y, Huang K, Chen X, Fu X, Dai W. Promoted effect of PANI on the preferential oxidation of CO in the presence of H_2 over Au/TiO_2 under visible light irradiation. Int J Hydrogen Energy 2014;39(32):18312–25.
[12] Kahlich MJ, Gasteiger HA, Behm RJ. Kinetics of the selective low-temperature oxidation of CO in H_2-rich gas over Au/α-Fe_2O_3. J Catal 1999;182:430–40. http://dx.doi.org/10.1006/jcat.1998.2333.
[13] Oliva D, Francesconi J, Mussati M, Aguirre P. Co-PrOx reactor design by model-bases optimization. J Power Sources 2008;182:307–16.
[14] Ayastuy JL, Gamboa NK, Gonzalez-Marcos MP, Gutierrez-Ortiz MA. CuO/CeO_2 washcoated ceramic monoliths for CO-PROX reaction. Chem Eng J 2011;171:224–31.
[15] Gómez LE, Tiscornia IS, Boix AV, Miró EE. Co/ZrO_2 catalysts coated on cordierite monoliths for CO preferential oxidation. Appl Catal A Gen 2011;401:124–33.
[16] Gómez LE, Tiscornia IS, Boix AV, Miró EE. CO preferential oxidation on cordierite monoliths coated with Co/CeO_2 catalysts. Int J Hydrogen Energy 2012;37:14812–9.
[17] Gómez LE, Boix AV, Miró EE. Co/ZrO_2, Co/CeO_2 and MnCoCe structured catalysts for COPrOx. Catal Today 2013;216:246–53.
[18] Barbato PS, Di Benedetto A, Landi G, Lisi L. CuO/CeO_2 based monoliths for CO preferential oxidation in H_2-rich streams. Chem Eng J 2015;279:983–93.
[19] Landi G, Barbato PS, Di Benedetto A, Lisi L. Optimization of the preparation method of CuO/CeO_2 structured catalytic monolith for CO preferential oxidation in H_2-rich streams. Appl Catal B Environ 2016;181:727–37.
[20] Amphelett JC, Mann RF, Peppley BA. On board hydrogen purification for steam reformation/PEM fuel cell vehicle power plants. Int J Hydrogen Energy 1996;21:673–8.
[21] Kahlich MJ, Gasteiger HA, Behm RJ. Kinetics of the selective CO oxidation in H_2-rich gas on Pt/Al_2O_3. J Catal 1997;171:93–105. http://dx.doi.org/10.1006/jcat.1997.1781.
[22] Venderbosch RH, Prins W, van Swaaij WPM. Platinum catalyzed oxidation of carbon monoxide as a model reaction in mass transfer measurements. Chem Eng Sci 1998;53:3355–66.
[23] Sedmak G, Hocevar S, Levec J. Kinetics of selective CO oxidation in excess of H_2 over the nanostructured $Cu_{0.1}Ce_{0.9}O_{2-y}$ catalyst. J Catal 2003;213:135–50. http://dx.doi.org/10.1016/S0021-9517(02)00019-2.

[24] Bollinger MA, Vannice MA. A kinetic and DRIFTS study of low-temperature carbon monoxide oxidation over Au-TiO catalysts. Appl Catal B Environ 1996;8:417–43.
[25] Cant NW, Ossipoff NJ. Cobalt promotion of Au/TiO_2 catalysts for the reaction of carbon monoxide with oxygen and nitrogen oxides. Catal Today 1997;36:125–33.
[26] Choi Y, Stenger HG. Kinetics, simulation and insights for CO selective oxidation in fuel cell applications. J Power Sources 2004;129:246–54.
[27] López E, Kolios G, Eigenberger G. Structured folded-plate reactor for CO preferential oxidation. Ind Eng Chem Res 2005;44:9659–67. http://dx.doi.org/10.1021/ie050282h.
[28] Laguna OH, Hernández WY, Arzamendi G, Gandía LM, Centeno MA, Odriozola JA. Gold supported on CuOx/CeO_2 catalyst for the purification of hydrogen by the CO preferential oxidation reaction (PROX). Fuel 2014;118:176–85.
[29] Yao L, Sethares WA. Nonlinear parameter estimation via the genetic algorithm. IEEE Trans Signal Process 1994;42:927–35.
[30] Routray K, Reddy KRSK, Deo G. Oxidative dehydrogenation of propane on V_2O_5/Al_2O_3 and V_2O_5/TiO_2 catalysts: understanding the effect of support by parameter estimation. Appl Catal A Gen 2004;265:103–13.
[31] Daneshpayeh M, Khodadadi A, Mostoufi N, Mortazavi Y, Sotudeh-Gharebagh R, Talebizadeh A. Kinetic modeling of oxidative coupling of methane over $Mn/Na_2WO_4/SiO_2$ catalyst. Fuel Process Technol 2009;90:403–10. http://dx.doi.org/10.1016/j.fuproc.2008.11.001.
[32] Jiang L, Xiao HH, He JJ, Sun Q, Gong L, Sun JH. Application of genetic algorithm to pyrolysis of typical polymers. Fuel Process Technol 2015;138:48–55. http://dx.doi.org/10.1016/j.fuproc.2015.05.001.
[33] Moreno MS, López E, Divins NJ, Llorca J. Parameter estimation of an empirical kinetic model for CO preferential oxidation. 43 JAIIO: Jornadas Argentinas de Informática, Simposio Argentino de Investigación Operativa (SIO 2014), Ciudad de Buenos Aires, Argentina.
[34] Brust M, Walker M, Bethell D, Schiffrin D, Whyman R. Synthesis of thiol-derivatised gold nanoparticles in a two-phase Liquid–Liquid system. J Chem Soc Chem Commun 1994;7:801–2. http://dx.doi.org/10.1039/C39940000801.
[35] Divins NJ, López E, Roig M, Trifonov T, Rodríguez A, González de Rivera F, et al. A million-channel CO-PrOx microreactor on a fingertip for fuel cell application. Chem Eng J 2011;167:597–602. http://dx.doi.org/10.1016/j.cej.2010.07.072.
[36] Rodriguez-Fernandez M, Egea JA, Banga JR. Novel metaheuristic for parameter estimation in nonlinear dynamic biological systems. BMC Bioinform 2006;7:483–501.
[37] Rangaiah GP. Stochastic global optimization techniques and applications in chemical engineering. Word Scientific Publishing; 2010.
[38] Marseguerra M, Zio E, Podofillini L. Model parameters estimation and sensitivity by genetic algorithms. Ann Nucl Energy 2003;30:1437–56.
[39] Seber GAF, Wild CJ. Nonlinear regression. John Wiley & Sons, Inc; 2003.
[40] Michalewicz Z. Genetic algorithms + data structures = evolutions programs. 3rd ed. Springer; 1996.
[41] Moles CG, Mendes P, Banga JR. Parameter estimation in biochemical pathways: a comparison of global optimization methods. Genome Res 2003;13:2467–74.
[42] Emig G, Klemm E. Technische chemie. 5th ed. Springer; 2005.
[43] Görke O, Pfeifer P, Schubert K. Kinetic study of ethanol steam reforming in a microreactor. Appl Catal A Gen 2009;306:232–41.
[44] Gonzo E. Conceptos básicos sobre lo fenómenos de transporte y transformación en catálisis heterogénea. 1st ed. Universidad Nacional de Salta; 2010.
[45] Gonzo E. Criteria for the estimation of transport effects in a network of heterogeneous catalytic reactions. Lat Am Appl Res 1993;23:1–9.
[46] Lin SD, Bollinger M, Vannice MA. Low temperature CO oxidation over Au/TiO_2 and Au/SiO_2 catalysis. Catal Lett 1993;17:245–62.